Hybrid Molecular Magnets Obtained by Insertion of Decamethylmetallocenium Cations into Layered, Bimetallic Oxalate Complexes: $[Z^{III}Cp^*_2][M^{II}M^{III}(ox)_3]$ (Z^{III} = Co, Fe; M^{III} = Cr, Fe; M^{II} = Mn, Fe, Co, Cu, Zn; ox = oxalate; Cp* = pentamethylcyclopentadienyl)

Eugenio Coronado,*[a] José-Ramón Galán-Mascarós,[a] Carlos-José Gómez-García,[a] Jürgen Ensling,[b] and Philipp Gütlich[b]

Abstract: A new series of hybrid organometallic–inorganic layered magnets with the formula $[Z^{III}Cp^*_2][M^{II}M^{III}(ox)_3]$ (Z^{III} = Co, Fe; M^{III} = Cr, Fe; M^{II} = Mn, Fe, Co, Cu, Zn; ox = oxalate; Cp* = pentamethylcyclopentadienyl) has been prepared. All of these compounds are isostructural and crystallize in the monoclinic space group *C*2/*m*, as found by X-ray structure analysis. Their structure consists of an eclipsed stacking of the bimetallic oxalate-based extended layers separated by layers of organometallic cations. These salts show spontaneous magnetization below T_c, which corresponds to the presence of ferro-, ferri-, or canted antiferromagnetism. Compounds in which the paramagnetic decamethylferrocenium is used instead of the diamagnetic decamethylcobaltocenium are good examples of chemically constructed magnetic multilayers with alternating ferromagnetic and paramagnetic layers. The physical properties of this series have been thoroughly studied by means of magnetic measurements and ESR and Mössbauer spectroscopy. We have found that the two layers are electronically quasiindependent. As a consequence, the bulk properties of these magnets have not been significantly affected by the insertion of a paramagnetic layer of $S = ½$ spins in between the extended layers. In fact, the critical temperatures remain unchanged even when comparing $[MCp^*_2]^+$ derivatives with $[XR_4]^+$ compounds (X = N, P; R = Ph, *n*Pr, *n*Bu). Nevertheless, the presence of the paramagnetic layer has been shown to have some influence on the hysteresis loops of these compounds. In the same context, the spin polarization of the paramagnetic units (which arises from the internal magnetic field created by the bimetallic layers in the ordered state) has been observed by Mössbauer and ESR spectroscopy.

Keywords: crystal engineering · decamethylferrocenium · layered magnets · magnetic properties · oxalate complexes

Introduction

Molecule-based magnets are the focus of much contemporary research in chemistry.[1] From a wise choice of constituent molecules, an extraordinary variety of magnets can be obtained that show original molecular architectures as well as interesting properties, or even a combination of properties. Especially noteworthy in this context are compounds that exhibit a layered structure, since these can be used to create new magnetic multilayered phases. These chemically designed, magnetic multilayered materials are crystalline compounds and therefore, have a higher degree of perfection than the magnetic multilayers obtained by deposition techniques and other physical methods. Furthermore, the layered structure should facilitate the insertion of molecules that can add complexity and interest to the resulting material.

An illustrative example of this class of materials is provided by the two-dimensional bimetallic phases (cation) $[M^{II}M^{III}(ox)_3]$ (M^{II} = Mn, Fe, Co, Cu, Zn ; M^{III} = Cr, Fe) first reported by Okawa et al. at the beginning of the 1990s,[2] which behave as ferro-,[3] ferri-,[4] or canted antiferromagnets[5] with critical temperatures ranging from 5 to 44 K. Their structure[6] consists of an extended anionic network formed by oxalate-bridged hexagonal layers of the two metal atoms. These bimetallic layers are separated by an organic counterion of the type $[XR_4]^+$ (X = N, P; R = Ph, *n*Pr, *n*Bu), which may act as a template controlling the formation of the net structure and thus determining the interlayer separation, as well as its packing.[6b] To increase the complexity of these phases one can replace this electronically "innocent" cation

[a] Prof. Dr. E. Coronado, Dr. C.-J. Gómez-García, Dr. J.-R. Galán-Mascarós
Departamento de Química Inorgánica
Universidad de Valencia
Dr. Moliner 50, 46100 Burjasot (Spain)
Fax: (+349) 6-386-4859
E-mail: eugenio.coronado@uv.es

[b] Prof. Dr. P. Gütlich, Dr. J. Ensling
Institut für Anorganische Chemie und Analytische Chemie
Johannes Gutenberg-Universität Mainz
Staudinger Weg 9, 55099 Mainz (Germany)

  0947-6539/00/0603-0552 $ 17.50+.50/0

by an electroactive one, with the aim of conferring a novel property, such as electrical conductivity, on the magnetic material. Our initial attempts to construct such hybrids with tetrathiafulvalene (TTF) molecules gave rise to the $[TTF]_4[M^{II}(H_2O)_2\{M^{III}(ox)_3\}_2]\cdot n\,H_2O$ family of semiconductors,[7] which is formed from layers of organic TTF molecules alternating with molecular layers of oxalate-bridged trimeric clusters. As the polymeric inorganic network was not maintained, no long-range magnetic order was observed in this family. A similar situation was encountered when the paramagnetic mononuclear complexes $[M^{III}(ox)_3]^{3-}$ (M = Fe, Cr) were combined with the bis(ethylenedithio)-TTF donor (BEDT-TTF). Interestingly, however, these hybrids exhibited superconducting properties in the organic component.[8] The first successful attempt to combine this organic donor with a polymeric bimetallic oxalato complex afforded the semiconducting hybrid salt $[BEDT\text{-}TTF]_2[CuCr(ox)_3]$.[9] The hybrid was obtained by electrocrystallization as a microcrystalline powder. Although all efforts to grow single crystals suitable for X-ray diffraction study have so far been unsuccessful, an extended bimetallic structure is formed in this case as demonstrated by the magnetic properties—the compound shows spontaneous magnetization as well as magnetic hysteresis below $T_c = 3$ K. Note that not only electrical properties can be incorporated into this bimetallic magnetic system, but also nonlinear optical properties can also be introduced by inserting organic dyes in between the layers.[10]

According to this hybrid approach we present here our attempts to prepare pure, magnetic multilayered materials with organometallic decamethylmetallocenium cations as counterions $[Z^{III}Cp^*_2]^+$ (Z^{III} = Fe, Co). In this case, two striking aspects will be studied: first, the possibility to construct multilayered crystalline architectures, in which ferro- or ferrimagnetic layers alternate with layers of dia- or paramagnetic species, and second, the effects produced on the magnetic properties of these hybrid magnets as a result of interactions between the two kinds of magnetic layers. A preliminary account of these multilayered magnets has already been published.[11]

Abstract in Spanish: *Se ha preparado una nueva serie de imanes híbridos organometálicos–inorgánicos estructurados en capas de fórmula $[Z^{III}Cp^*_2][M^{II}M^{III}(ox)_3]$ (Z^{III} = Co, Fe; M^{III} = Cr, Fe; M^{II} = Mn, Fe, Co, Cu, Zn; ox = oxalato; Cp* = pentametilciclopentadienilo). Todos estos compuestos son isoestructurales, cristalizan en el grupo espacial monoclínico C2/m, como se comprobó por difracción de rayos-X, y su estructura está formada por un apilamiento eclipsado de capas extendidas basadas en complejos bimetálicos de oxalato separadas por capas de los cationes organometálicos. Estas sales presentan magnetización espontánea por debajo de T_c, que se corresponde con la presencia de ferro-, ferri- o débil ferromagnetismo. Cuando se utiliza el catión paramagnético decametilferricinio en lugar del diamagnético decametilcobalticinio, estos compuestos son un buen ejemplo de sistemas magnéticos multicapa construídos químicamente, con capas ferromagneticas y paramagnéticas alternadas. Las propiedades físicas de esta serie de compuestos han sido estudiadas con detalle por medio de medidas magnéticas y espectroscopías RSE y Mössbauer. Se ha observado que ambas subredes son quasi-independientes desde el punto de vista electrónico, por lo que las propiedades de estos imanes no se ven modificadas significativamente por la inserción de una capa paramagnética de spines S = ½ entre las capas extendidas. De hecho, las temperaturas críticas no presentan cambios apreciables si comparamos los derivados de $[MCp^*_2]^+$ con los de $[XR_4]^+$. Sin embargo, la presencia de una capa paramagnética sí que tiene influencia en los ciclos de histéresis de estos compuestos. Además, la polarización de las unidades paramagnéticas por medio del campo magnético interno generado por las capas bimetálicas en el estado ordenado ha podido ser observada por espectroscopía Mössbauer y RSE.*

Results and Discussion

Synthesis and structure: A total of sixteen compounds divided into two different series, namely the decamethylferrocenium series $[FeCp^*_2][M^{II}M^{III}(ox)_3]$ (M^{III} = Cr; M^{II} = Mn, Fe, Co, Cu, Zn. M^{III} = Fe; M^{II} = Mn, Fe, Zn), and the corresponding decamethylcobaltocenium series $[CoCp^*_2][M^{II}M^{III}(ox)_3]$ were synthesized by addition of a solution of the cation (in water, or DMF in the case of decamethylcobaltocenium) to an aqueous solution of the tris-oxalate complex of the trivalent metal with an excess of the divalent metal. The excess of divalent metal was crucial, since the stoichiometric reaction did not yield any successful results. A Ni^{II} derivative was also prepared by the same procedure, but X-ray powder diffraction demonstrated that it is indeed a different structural phase, although it does possess magnetic ordering. (Single crystals of this phase have not yet been obtained.) It is also of interest to mention that our attempts to use the same synthetic procedure for the ferrocenium cation, $[FeCp_2]^+$, were unsuccessful, possibly because it is not big enough to stabilise the formation of the layered bimetallic oxalate-based network.

The compounds were obtained as green or yellow microcrystals and were all isostructural as demonstrated by X-ray powder diffraction. The monoclinic unit cell parameters are summarized in Table 1. For two compounds of the $[FeCp^*_2]$ series, namely $Mn^{II}Cr^{III}$ and $Mn^{II}Fe^{III}$, single crystals suitable for X-ray diffraction analysis were obtained by slow diffusion of a dilute aqueous decamethylferrocenium solution into another aqueous solution containing the $[M^{III}(ox)_3]^{3-}$ ion and an excess of the divalent metal. The structure consists of anionic layers of the well-known honeycomb, bimetallic, oxalato-bridged network with decamethylferrocenium cations intercalated in between (Figure 1, top). The most striking feature of this structure, in comparison with most of the $[XR_4]^+$ derivatives, is related to the stacking of the anionic layers. In this case all the bimetallic layers are of the same type and are eclipsed with respect to each other creating hexagonal channels running along the *c* axis, instead of a graphite-like arrangement. The organometallic cations exhibit the staggered configuration (symmetry D_{5d}) and are located at the center of the hexagonal channels to give a pseudohexagonal two-dimensional (2D) packing. These cations are tilted with

Table 1. Unit cell parametrers for the series $[Z^{III}Cp^*_2][M^{II}M^{III}(ox)_3]$.

$Z^{III}M^{II}M^{III}$	a [Å]	b [Å]	c [Å][b]	β [°]	V [Å^3]
FeMnCr[a]	8.94(3)	17.10(2)	9.282(10)	93.3(2)	1417(6)
FeFeCr	8.875(13)	16.96(3)	9.44(2)	93.02(14)	1420(10)
FeCoCr	8.82(2)	17.00(6)	9.58(3)	92.7(3)	1434(9)
FeCuCr	8.82(9)	17.1(2)	9.69(14)	94(1)	1500(100)
FeZnCr	8.84(3)	17.05(7)	9.65(8)	92.7(3)	1454(9)
FeMnFe[a]	9.0645(8)	17.143(3)	9.215(4)	93.66(2)	1429(1)
FeFeFe	8.920(7)	17.0738(11)	9.334(9)	93.14(8)	1419(5)
FeZnFe	8.95(3)	17.13(4)	9.35(4)	93.2(2)	1430(40)
CoMnCr	8.926(10)	17.12(2)	9.26(2)	94.08(9)	1411(9)
CoFeCr	8.94(2)	17.09(6)	9.44(4)	93.8(3)	1440(20)
CoCoCr	9.03(6)	17.0(2)	9.36(7)	93.2(5)	1430(70)
CoCuCr	8.98(4)	17.00(14)	9.40(7)	93.5(5)	1430(50)
CoMnFe	9.15(3)	17.23(4)	9.25(3)	94.3(2)	1450(40)
CoFeFe	8.94(2)	17.09(4)	9.28(3)	94.0(2)	1410(20)

[a] Parameters obtained by single-crystal X-ray diffraction. [b] This parameter (c) corresponds to the interlayer separation (d).

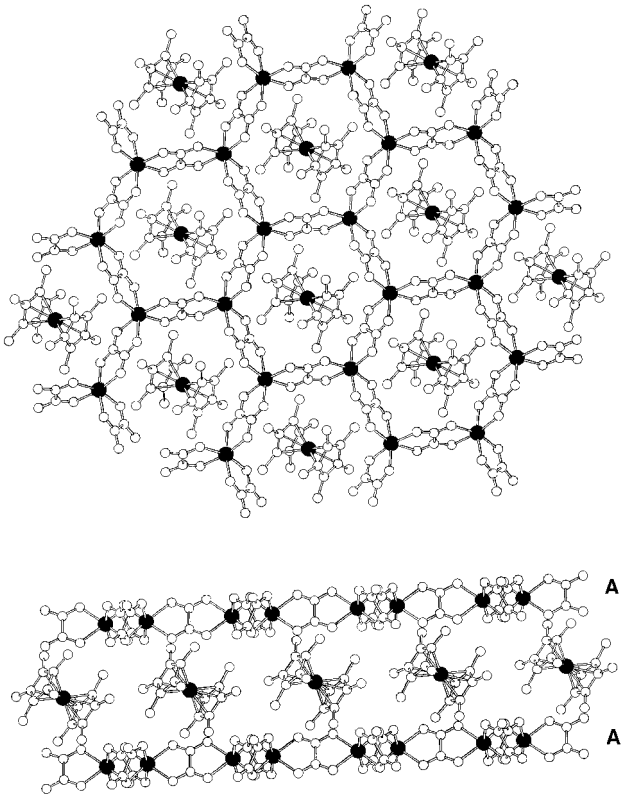

Figure 1. Two views of the structure of $[FeCp^*_2][MnFe(ox)_3]$: in the *ab* plane (top) and in the *ac* plane (bottom).

respect to the anionic layer by 32.6°(angle defined by the fivefold symmetry axis of the cation with the normal to the bimetallic plane) such that the two pentamethylcyclopentadienyl molecules of each $[FeCp^*_2]^+$ ion are pointing towards the center of the hexagons of two adjacent layers (Figure 1, bottom). The interlayer separation is in the range 9.2 – 9.7 Å, similar to that found in previous compounds of the 2D phases, and there is no evidence of hydrogen-bond interactions between the cations and the layers (the minimum H ··· O distance is 2.58 Å). A second distinctive feature of this structure with respect to the other structurally known 2D phases is that now the cation does not penetrate into the honeycomb net (the minimum distance of the cation to this plane is 0.88 Å; the distance from the mean plane defined by the metals to the closest hydrogen from a methyl group). This suggests that the "templating" effect of the cation is not necessary for the formation of the honeycomb layer.

Magnetic measurements:

Decamethylcobaltocenium salts: The magnetic susceptibilities of all the compounds of the $[CoCp^*_2]^+$ series closely resemble those of the corresponding $[XR_4]^+$ salts. Thus, in the paramagnetic region the Cr^{III} compounds show ferromagnetic interactions between neighboring Cr^{III} and M^{II} ions, as indicated by the positive values of the Weiss constants (Table 2). In turn, in the Fe^{III} compounds the near-neighbor exchange interactions are antiferromagnetic, with large negative values of the Weiss constants (Table 2). The similarity to the $[XR_4]^+$ salts is also evident in the low-temperature region, in which the Cr^{III} derivatives show an abrupt increase in magnetization at temperatures below 15 K, corresponding to the onset of long-range order (Figure 2, top), while in the Fe^{III} compounds the onset of long-range order occurs at higher temperatures (around 25 and 45 K for $Mn^{II}Fe^{III}$ and $Fe^{II}Fe^{III}$, respectively) (Figure 2, bottom). In the case of $Mn^{II}Fe^{III}$ a broad maximum in χ near 50 K is also observed, indicating the presence of low-dimensional antiferromagnetism. In the ordered state the magnetic properties of these two compounds are sharply different. Thus, the magnetization of $Mn^{II}Fe^{III}$ increases gradually below 10 K, but in $Fe^{II}Fe^{III}$ it decreases steadily down to 10 K and becomes strongly negative below 20 K.

The appearance of magnetic ordering has been also checked by AC magnetic measurements, which have allowed us to estimate more precisely the critical temperatures. In

Table 2. Magnetic parameters for the series $[CoCp^*_2][M^{II}M^{III}(ox)_3]$, $[FeCp^*_2][M^{II}M^{III}(ox)_3]$ and $[NBu_4][M^{II}M^{III}(ox)_3]$[a]: critical temperature (T_c), Weiss constant (Θ), Curie constant (C), saturation magnetization (M_S), remnant magnetization at 2 K (M_R) and coercive field at 2 and 5 K (H_{coer}).

$M^{II}M^{III}$	$[CoCp^*_2]$							$[FeCp^*_2]^+$							$[NBu_4]^+$	
	T_c [K]	Θ [K]	C [emu K mol^{-1}]	M_S [μ_B]	M_R [μ_B]	H_{coer} [kG] [2 K]	[5 K]	T_c [K]	Θ [K]	C [emu K mol^{-1}]	M_S [μ_B]	M_R [μ_B]	H_{coer} [kG] [2 K]	[5 K]	T_c [K]	H_{coer} [kG] [5 K]
MnCr	5.1	7.3	6.23	7.0	0.3	0.04	–	5.3	10.1	6.61	8.09	0.15	0.02	0.01	6	0.02
FeCr	12.7	13.6	5.26	4.6	3.5	1.94	0.76	13.0	12.3	6.35	6.20	3.60	1.10	0.33	12	0.32
CoCr	8.2	9.9	5.08	5.0	1.3	0.25	0.05	9.0	11.4	4.77	5.50	1.20	0.13	0.05	10	0.08
CuCr	6.7	18.1	2.10	3.6	1.7	0.20	0.02	7.0	15.8	2.88	4.90	1.50	0.18	0.04	7	0.03
MnFe	25.4	– 95.9	8.50	0.4	< 0.01	0.15	0.15	28.4	– 80.8	9.13	1.34	0.10	0.12	0.04	28	–
FeFe	44.0	– 84.9	7.14	0.5	< 0.01	0.10	0.10	43.3	– 67.1	7.99	1.40	0.02	0.37	1.24	45	–

[a] Data from ref. [3] for Cr^{III} derivatives and ref. [5b] for Fe^{III} derivatives.

0947-6539/00/0603-0554 $ 17.50+.50/0 *Chem. Eur. J.* **2000**, *6*, No. 3

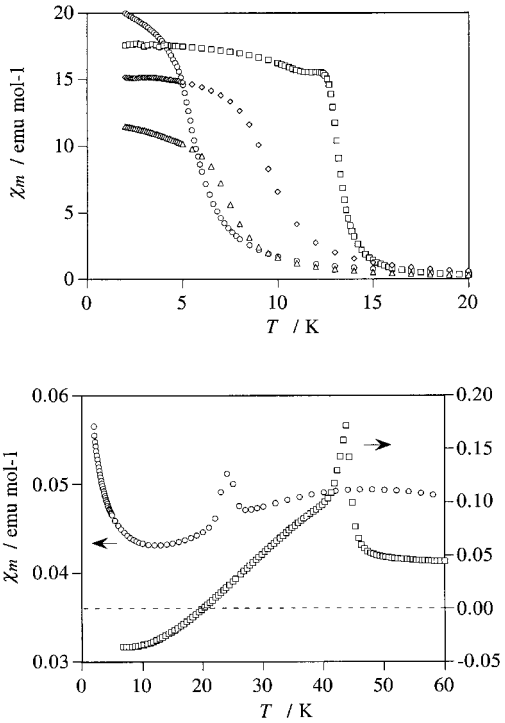

Figure 2. Plot of χ_m vs T for the $[CoCp_2^*][M^{II}Cr(ox)_3]$ (top) and $[CoCp_2^*][M^{II}Fe(ox)_3]$ (bottom) series. M^{II} = Mn (○), Fe (□), Co(◇), Cu(△).

both the Cr^{III} and the Fe^{III} derivatives, the AC data show a sharp peak in the in-phase signal at a given temperature that defines T_c, accompanied by an out-of-phase signal below T_c (Figure 3). In the Cr^{III} series the critical temperatures estimated in this way range from 5.1 to 12.7 K (Table 2). In

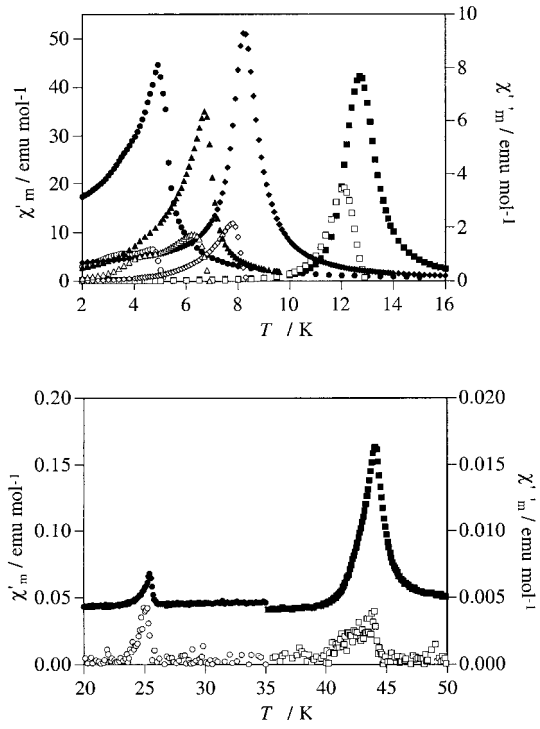

Figure 3. AC susceptibility measurements for the $[CoCp_2^*][M^{II}Cr(ox)_3]$ (top) and $[CoCp_2^*][M^{II}Fe(ox)_3]$ (bottom) series. Solid symbols represent in-phase signals, and open symbols the out-of-phase signal. M^{II} = Mn (●), Fe (■), Co(◆), Cu(▲).

such a case the nature of the magnetic transition corresponds to a ferromagnetic ordering, as demonstrated by the field dependence of the isothermal magnetization performed at 2 and 5 K. In fact, one observes a rapid saturation of the magnetization with M_S values that are compatible with a parallel alignment of the interacting spins (Figure 4, top). However, the magnetic field required to reach the saturation

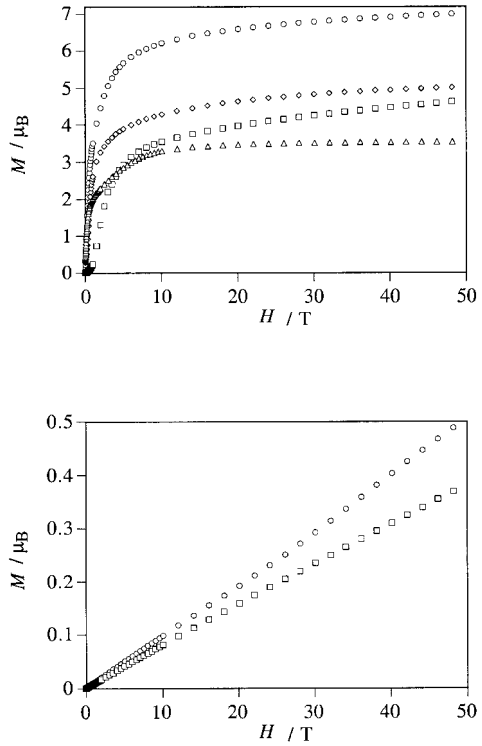

Figure 4. Plot of magnetization vs applied field for the $[CoCp_2^*][M^{II}Cr(ox)_3]$ (top) and $[CoCp_2^*][M^{II}Fe(ox)_3]$ (bottom) series. M^{II} = Mn (○), Fe (□), Co(△), Cu(◇).

is rather large, and furthermore, the M_S values are slightly smaller than expected. This feature has already been noted in the $[NBu_4]^+$ salts and has been attributed to the presence of a spin canting in the ferromagnetic structure.[3] Below T_c these ferromagnets exhibit magnetic hysteresis with coercive fields of up to 2000 G. The magnetic parameters for this series are summarized in Table 2. An anomalous magnetization curve has been observed in the $Fe^{II}Cr^{III}$ derivative. At low fields the magnetization tends to be close to zero, and only above 10^3 G does it increase sharply up to 10^4 G; at higher fields the magnetization increases gradually without reaching saturation. As a consequence, the magnetization at 5 T is still small compared with the expected M_S value (4.6 compared with 7 μ_B). This effect is too strong to be attributed to a spin canting. In the present case it is more probably due to the presence of a small amount of Fe^{III} ions as they should introduce competing antiferromagnetic interactions in the ferromagnetic layer. In fact, Mössbauer spectroscopy has shown there to be 15% of Fe^{III} ions (see below).

In the Fe^{III} series the observation of a sharp peak in the in-phase AC susceptibility indicates a phase transition to a magnetically ordered state at 44.0 K for $Fe^{II}Fe^{III}$ and at 25.4 K

for $Mn^{II}Fe^{III}$. The fact that this signal is accompanied by an out-of-phase signal at the same temperature indicates that in the ordered state the antiferromagnetic coupling is unable to cancel the two magnetic moments. In the compound $Fe^{II}Fe^{III}$ the ordered state should be ferrimagnetic as the two antiparallel spins are unequal ($S_{Fe^{III}} = 5/2$, $S_{Fe^{II}} = 2$). In turn, in the compound $Fe^{III}Mn^{II}$ the two spins are equal ($S_{Fe^{III}} = S_{Mn^{II}} = 5/2$), so a spin canting should be present in this antiferromagnet. The field-dependent magnetization (Figure 4, bottom) shows in both cases a linear increase, with very small values at 5 T which are consistent with the proposed magnetic orderings. A small hysteresis with coercive fields of about 150 and 100 G at 2 K is also observed.

Finally, the $Zn^{II}Cr^{III}$ and $Zn^{II}Fe^{III}$ compounds show paramagnetic behavior in good agreement with the structure in which the diamagnetic Zn^{II} ions isolate the Cr^{III} and Fe^{III} ions in the two-dimensional network.

Decamethylferrocenium derivatives: When the diamagnetic $[CoCp_2^*]^+$ ion is substituted by the paramagnetic $[FeCp_2^*]^+$ ion we end up with a material in which two kinds of magnetic sublattices alternate in the structure. As a consequence of the mutual interactions between these two magnetic sublattices, two types of changes in the magnetic properties can be anticipated.

1) A change in the bulk properties of the bimetallic magnetic layers due to the presence of the inserted paramagnetic cations.
2) A change in the electronic properties of the paramagnetic cations as a consequence of the internal magnetic field created by the bimetallic layers in the ordered state. For example, in the ordered state the bimetallic magnetic layers are expected to polarize the spins of the metallocene layer and therefore, a Zeeman splitting of the $S = 1/2$ spins of the paramagnetic cations may be observed by local techniques such as Mössbauer or ESR spectroscopy.

In relation to the former point we observe that, in general, the magnetic properties of all these compounds are similar to those observed in the decamethylcobaltocenium salts, as demonstrated by the magnetic parameters summarized in Table 2. The susceptibility and magnetization measurements are approximately the sum of the magnetic contributions from the two kinds of magnetic sublattices. Apparently, the structural changes imposed by the decamethylmetallocenium cations, and the presence of paramagnetic units in between the 2D bimetallic layers have no significant effects on the magnetic ordering of these molecule-based magnets. In fact, the critical temperatures remain roughly the same for each $M^{II}M^{III}$ pair when compared with those found for the tetraalkylammonium salts (Table 2). Only in the $Mn^{II}Fe^{III}$ derivatives does T_c change by several Kelvin, but similar changes had already been observed in different tetraalkylammonium salts. These results indicate that the two magnetic sublattices essentially behave independently with the magnetic ordering being mainly controlled by the bimetallic oxalate network. Nevertheless, some influence of the insertion of the metallocene cations between the magnetic layers is observed in the magnetic properties of the ordered state, that is, in the hysteresis loops. Thus, substitution of $[CoCp_2^*]^+$ by the paramagnetic $[FeCp_2^*]^+$ produces noticeable changes in the coercive fields. For example, H_{coer} at 2 K decreases in the $Fe^{II}Cr^{III}$ derivatives from 1940 to 1100 G, whereas it decreases in the $Co^{II}Cr^{III}$ compounds from 250 to 130 G (Table 2). These changes must be attributed to the presence of the paramagnetic complex, as the structural features in the two series are the same, and other factors, such as the size of the particles, do not seem to have any influence in these materials. In fact, the homogeneous particle size of all the samples was checked by electron microscopy; grinding the compounds produced no significant changes in coercivity. For example, in the $[CoCp_2^*]$ derivatives the value of H_{coer} remains constant within experimental error when grinding the sample from the original particle size (2–5 μm) to 0.2–0.5 μm. Interestingly, in the $[XR_4]^+$ series the coercive fields are close to those observed for the $[FeCp_2^*]^+$ group. In this case it seems that the effect of the presence of paramagnetic units is compensated by the different packing of the oxalato layers.

Another remarkable result in this series is the presence of a negative magnetization for the $Fe^{II}Fe^{III}$ derivatives. This behavior had already been observed for some $[XR_4]^+$ derivatives,[5b] and is typical of a type-N ferrimagnet, according to Néel's classification.[12] This phenomenon can arise when the two sublattices of a ferrimagnet have a different temperature dependence. In this particular case, since the Fe^{III} ground state is orbitally nondegenerate, the magnetization of the Fe^{III} sublattice should follow a Brillouin curve in the molecular field approximation, but that of the Fe^{II} will not, as it has an orbitally degenerate ground state. Evidence for this comes from Mössbauer spectroscopy as presented below. The compensation temperature changes from 20 to 27 K when one passes from the $[CoCp_2^*]^+$ to the $[FeCp_2^*]^+$ derivative. This indicates that the presence of the paramagnetic units in between the ferrimagnetic layers has a real effect upon the magnetically ordered state in these materials.

Mössbauer spectroscopy: ^{57}Fe Mössbauer spectroscopy is a very useful tool for studying the electronic, magnetic, and lattice-dynamic properties of these molecular magnets. It has already been used to study the iron-containing $[XR_4]^+$ derivatives.[13] In our case, the insertion of $[FeCp_2^*]^+$ in between the magnetic layers adds versatility to these magnets. The characteristic spectrum of the paramagnetic cation $[FeCp_2^*]^+$ measured in the salt $[FeCp_2^*][BF_4]$ shows a broad asymmetric band centered at 0.46 mm s^{-1} that can be fitted to two Lorentzian lines (Figure 5, top). When $[FeCp_2^*]^+$ is inserted into the layered structure of the paramagnet $Zn^{II}Cr^{III}$, the Mössbauer spectrum is still roughly the same in the overall range of temperatures (1.8–300 K) (Figure 5, bottom). In order of complexity, the next step is to study the spectra of the compounds containing $[FeCp_2^*]^+$ inserted in the ferromagnetic layers $Mn^{II}Cr^{III}$, $Co^{II}Cr^{III}$ (Figure 6) and $Cu^{II}Cr^{III}$, as these magnets do not contain iron atoms in the bimetallic layer. The characteristic resonance line associated with $[FeCp_2^*]^+$ is observed above T_c. Below T_c this band becomes weaker and its base broadens in such a way that it can no longer be fitted to the initial parameters. This corresponds to the spectrum of a Zeeman-split nuclear spin $I = 3/2$ due to fast relaxation processes, which means that the fluctuation in the electronic

0947-6539/00/0603-0556 $ 17.50+.50/0 *Chem. Eur. J.* **2000**, *6*, No. 3

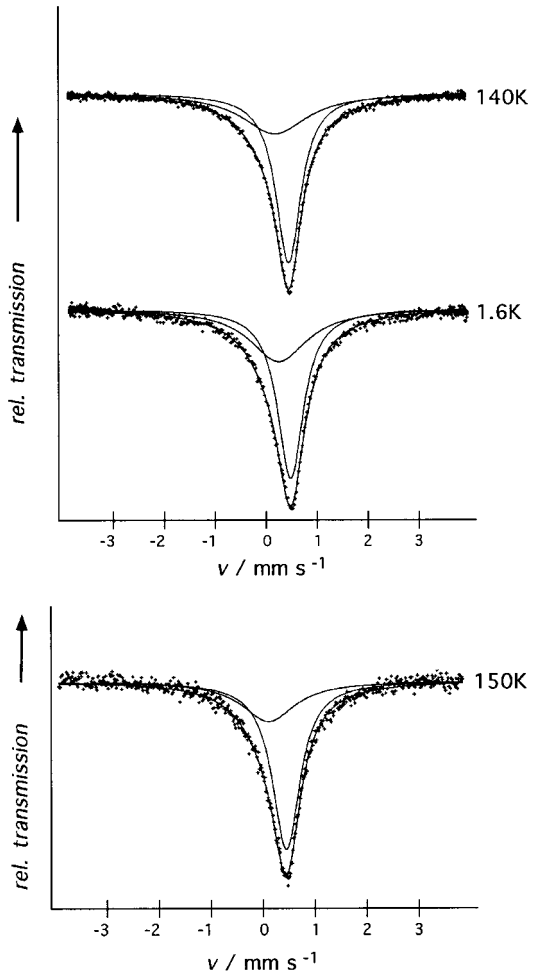

Figure 5. Mössbauer spectra of the $[FeCp_2^*][BF_4]$ salt at two different temperatures (top) and Mössbauer spectrum of the $[FeCp_2^*][ZnCr(ox)_3]$ derivative (bottom).

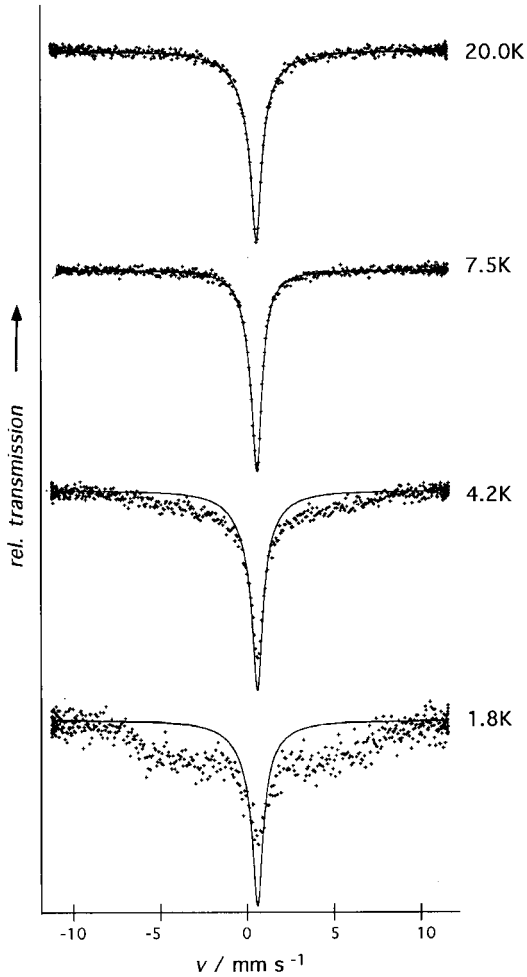

Figure 6. Mössbauer spectra of the $[FeCp_2^*][CoCr(ox)_3]$ derivative at different temperatures.

spin $S = ½$ between $M_S = ½$ and $M_S = -½$ is faster than the Mössbauer time scale ($> 10^{-7}$ s), and so the time-averaged magnetic field "seen" by the nucleus is zero. At very low temperatures (1.8 K) the spectra are more complicated as the relaxation processes become slower, but even at these temperatures the magnetic hyperfine spectra are not resolved. According to these results, it is evident that the spin of the $[FeCp_2^*]^+$ is polarized by the internal magnetic field generated by the bimetallic layers below T_c, although fast relaxation processes prevent clear observation of the corresponding sextet. Thus, additional information such as the value of the internal magnetic field cannot be extracted. The fast relaxation processes can be attributed to two factors, namely, the relatively low values of T_c in these materials, and the good screening provided by the diamagnetic pentamethylcyclopentadienyl ligands acting over the iron nucleus.

The spectra observed in the above case contrast with those obtained when iron is present in the bimetallic layer. The simplest case is provided by the $Fe^{II}Cr^{III}$ compound (Figure 7), where the spectrum at high temperatures shows, in addition to the characteristic signal from $[FeCp_2^*]^+$, a quadrupolar doublet with the typical parameters of a high-spin Fe^{II} ($\delta =$ 1.19 and $\Delta E_Q = 1.98$ mm s^{-1} at 20 K). Below T_c (13 K) the presence of an internal magnetic field leads to a splitting of this doublet into a doublet and a triplet ($H_{int} = 65$ kG at 4.2 K), which is the typical multiplet expected for a high-spin Fe^{II} ion; the $[FeCp_2^*]^+$ band shows a relaxation spectrum similar to that of the previous case. The most complex spectrum is that of compound $Fe^{II}Fe^{III}$ (Figure 8), as it contains three different iron sites. At high temperatures, a singlet and two doublets are observed. The singlet is the characteristic band of $[FeCp_2^*]^+$. One of the doublets is very similar to that found in $Fe^{II}Cr^{III}$, so it corresponds to a high-spin Fe^{II} ion. The other doublet exhibits a smaller isomer shift and quadrupolar splitting ($\delta = 0.45$ and $\Delta E_Q = 0.37$ mm s^{-1} at 45 K) and can be assigned to high-spin Fe^{III}. Observation of these two signals indicates that the Fe^{II}/Fe^{III} network is a "trapped-valence system" where the electron transfer rate between the two iron species is less than the Mössbauer time scale ($< 10^7$ s^{-1}). Just below T_c (44 K) the shape of the spectrum becomes more complicated and the bands are broadened. The complexity increases further as the temperature is lowered, and the spectrum shows a number of absorption lines spreading over a wide energy range. For example, at 40 K the spectrum can be understood as the superposition of the absorptions of the magnetically split high-spin Fe^{II} and Fe^{III} ions from the anionic layer and the

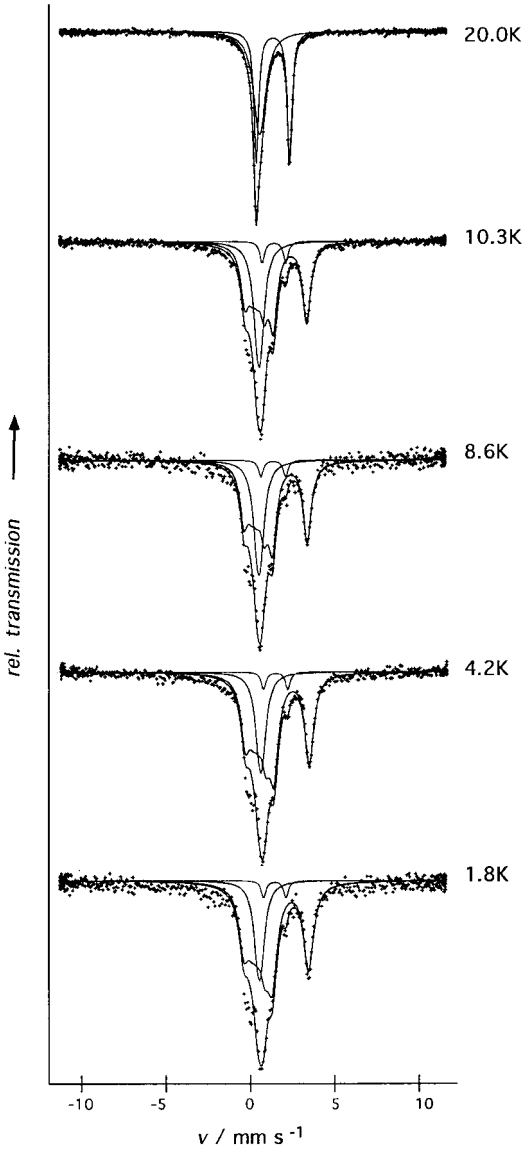

Figure 7. Mössbauer spectra of the $[FeCp_2^*][FeCr(ox)_3]$ derivative at different temperatures.

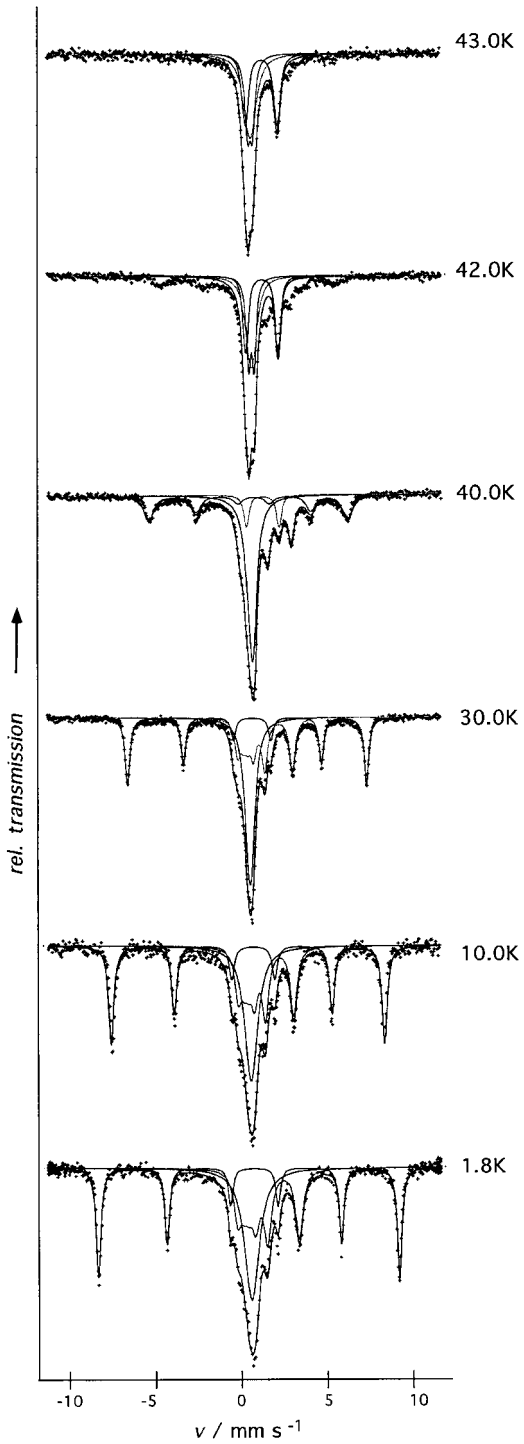

Figure 8. Mössbauer spectra of the $[FeCp_2^*][FeFe(ox)_3]$ derivative at different temperatures.

relaxation absorption of the low-spin $[FeCp_2^*]^+$. The evolution of this spectrum as a function of the temperature is very interesting because the two Fe ions of the anionic layer behave differently. Thus, at 40 K all the high-spin Fe^{III} ions show a nuclear Zeeman splitting, and no trace of the original doublet is observed. Upon further cooling, the internal magnetic field increases until it saturates at around 10 K to reach a value typical for this kind of ion (550 kG). In contrast, at this temperature (40 K) only some of the high-spin Fe^{II} ions ($\approx$70%) show a nuclear Zeeman splitting, and only at 30 K does the original doublet disappear completely. The internal magnetic field expected for a high-spin Fe^{II} saturates below 10 K (65 kG). In view of the fact that the biggest contribution to the internal magnetic field "seen" by the Fe^{II} nucleus comes from the surrounding nearest neighbours (3 Fe^{III} ions), and vice versa, the above result confirms that in the $Fe^{II}Fe^{III}$ oxalate-based anionic layer the magnetization for the Fe^{II} sublattice increases faster than that for the Fe^{III} sublattice. This evolution accounts for the negative magnetization observed in the magnetic measurements below the compensation point.[14] Focusing on the signal from $[FeCp_2^*]^+$, we notice that, although in this case T_c is much higher than in the Cr^{III} derivatives, the same relaxation behavior is found as in other compounds. Even at very low temperatures the relaxation is too fast to observe the hyperfine magnetic splitting. Thus, the presence of a fast spin-flip for the electronic spin of decamethylferrocenium may suggest that

0947-6539/00/0603-0558 $ 17.50+.50/0 *Chem. Eur. J.* **2000**, *6*, No. 3

the magnetic ordering in these materials has strong 2D character.

Mössbauer spectroscopy has also been useful in studying the compound $[CoCp_2^*][FeCr(ox)_3]$. In addition to the doublet from the high-spin Fe^{II} ion ($\delta = 1.18$ and $\Delta E_Q = 1.96\ mm\,s^{-1}$ at 20 K), its spectrum (Figure 9) shows a weak signal corresponding to the presence of some impurities of high-spin Fe^{III} ($\approx 15\,\%$). This last signal displays a hyperfine

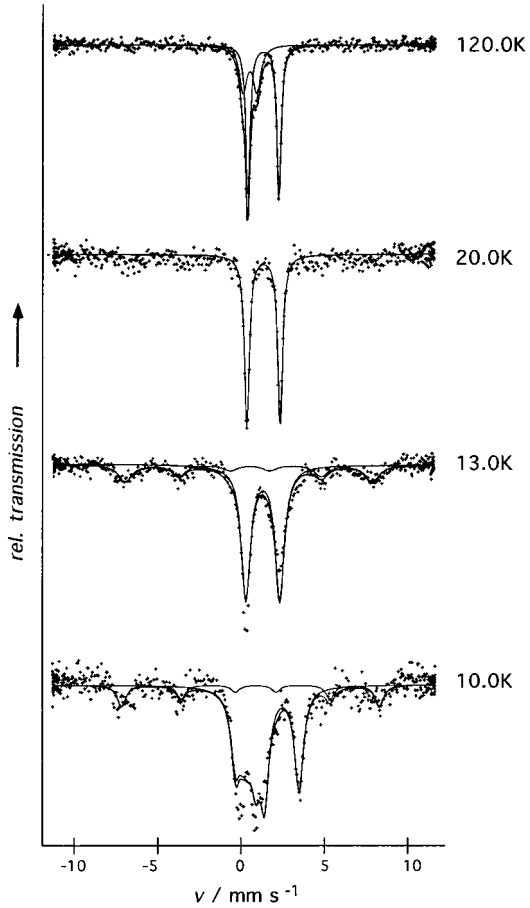

Figure 9. Mössbauer spectra of the $[CoCp_2^*][FeCr(ox)_3]$ derivative at different temperatures.

magnetic splitting below 60 K, while the hyperfine magnetic splitting for the Fe^{II} ions is observed only below T_c (13 K). As a result, a topological disorder does appear in the anionic network since some of the Fe^{II} sites are randomly substituted by Fe^{III}. From a magnetic point of view such a disorder should introduce antiferromagnetic $Fe^{III}Cr^{III}$ interactions into the ferromagnetic layer $Fe^{II}Cr^{III}$. This accounts for the anomalous magnetic properties observed in this material (see above). The origin of this impurity is related to partial oxidation of Fe^{II} during synthesis, and since it does not appear in the decamethylferrocenium derivative, it should be related to the different synthetic route, and in particular, to the use of DMF as solvent. So, a purely aqueous route could prevent the occurrence of Fe^{III} in the network.

ESR spectroscopy: The Zeeman splitting of the $S = ½$ spins of the paramagnetic $[FeCp_2^*]^+$ ions produced by the ferro- or ferrimagnetic anionic layers has been confirmed by ESR spectroscopy. The typical spectrum of $[FeCp_2^*]^+$ at low temperatures (below 50 K) shows an anisotropic signal with $g_\parallel = 4.45$ and $g_\perp = 1.02$ (Figure 10). The best way to monitor the evolution of this signal is to study those derivatives in which the bimetallic magnetic network is ESR-silent or shows signals at fields different from those observed in the $[FeCp_2^*]^+$ spectrum. In view of the spectra obtained for the decamethylcobaltocenium salts, we chose to study the decamethylferrocenium salts of $Fe^{II}Cr^{III}$, $Mn^{II}Cr^{III}$, and $Mn^{II}Fe^{III}$.

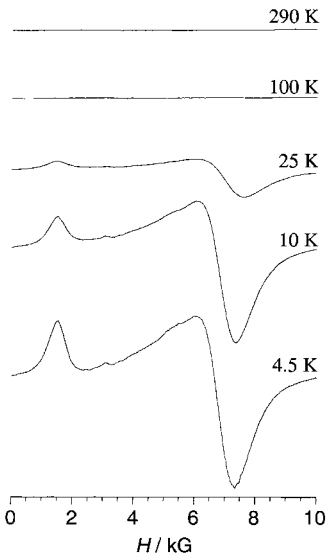

Figure 10. ESR spectra of the $[FeCp_2^*][BF_4]$ salt at different temperatures.

The magnetic layer of $Fe^{II}Cr^{III}$ is ESR-silent. Accordingly, the spectrum at 15 K of the ferromagnet $[FeCp_2^*][Fe^{II}Cr^{III}(ox)_3]$ is very similar to that found in the $[BF_4]^-$ salt (Figure 11) with $g_\parallel = 4.64$ and $g_\perp = 1.05$. Below the temperature of the ferromagnetic transition (13 K), $g_\perp$ moves towards lower magnetic fields (from 8000 G at 15 K to 3500–4000 G at 4.3 K) making the signal less anisotropic. This g-shift demonstrates that below T_c the $S = ½$ spin of the $[FeCp_2^*]^+$ unit "sees" the internal magnetic field of the ferromagnet. This internal field is added to the applied

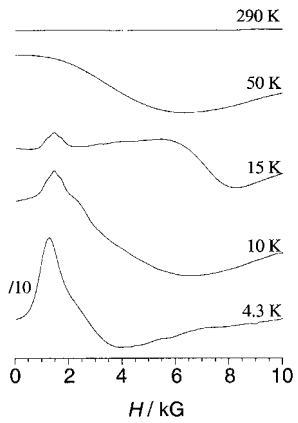

Figure 11. ESR spectra of the $[FeCp_2^*][FeCr(ox)_3]$ derivative at different temperatures.

magnetic field so as to decrease the resonance field. The same effect is found in the ferromagnetic compound $[FeCp_2^*][Mn^{II}Cr^{III}(ox)_3]$ (Figure 12). The only signal seen from the decamethylferrocenium species below 20 K in this case is a bump corresponding to $g_\perp$. This signal is about 100 times less intense than the signal associated with the anionic layers. Below T_c ($\approx$6 K), $g_\perp$ moves towards lower magnetic fields (from 8000 G at 10 K to 4000 G at 4.2 K) and is superimposed on the main signal at 4.2 K.

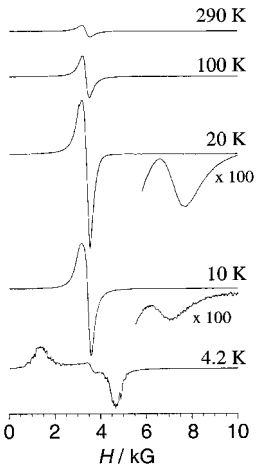

Figure 12. ESR spectra of the $[FeCp_2^*][MnCr(ox)_3]$ derivative at different temperatures.

For the compound $[FeCp_2^*][Mn^{II}Fe^{III}(ox)_3]$ (Figure 13, right) the signal associated with the bimetallic anionic network is an isotropic band centered around $g = 2.0$, which decreases in intensity upon cooling (Figure 13, left) in agreement with the antiferromagnetic coupling between the two interacting $S = 5/2$ spins. At low temperatures (below 20 K) this signal becomes very weak and the paramagnetic signal from the $[FeCp_2^*]^+$ unit dominates, which facilitates the study of its thermal evolution. As in the other cases, in the ordered phase (below 25 K) $g_\perp$ moves towards lower magnetic fields upon cooling. However, in this instance the shift is smaller. Thus, at 4.2 K the $g_\perp$ signal is centered around 6000 G, while in the previous two cases it was centered over the range 3500–4000 G. This result is in agreement with the fact that $[FeCp_2^*][Mn^{II}Fe^{III}(ox)_3]$ is a weak ferromagnet, and so the internal magnetic field generated by this magnet is smaller than those produced by the ferromagnets $[FeCp_2^*][Mn^{II}Cr^{III}(ox)_3]$ and $[FeCp_2^*][Fe^{II}Cr^{III}(ox)_3]$.

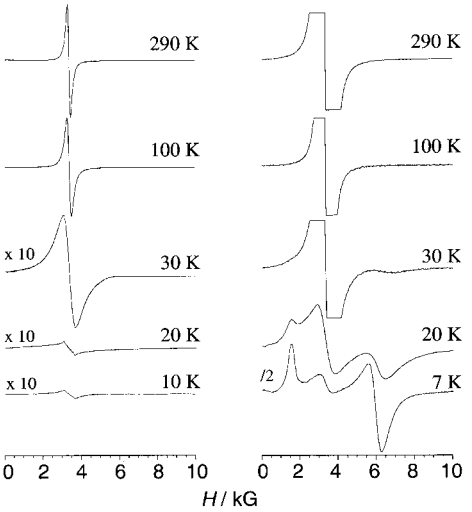

Figure 13. ESR spectra of the $[CoCp_2^*][MnFe(ox)_3]$ derivative (left) compared with the ESR spectra of the $[FeCp_2^*][MnFe(ox)_3]$ derivative (right) at different temperatures.

Conclusion

In this article we have shown how anionic layers based on bimetallic oxalate complexes can be used as inorganic hosts for organometallic cations in order to construct new multilayered hybrid magnets. We have found that an organometallic monocation, such as decamethylferrocenium $[FeCp_2^*]^+$ and decamethylcobaltocenium $[CoCp_2^*]^+$, stabilizes the honeycomb bimetallic layer, in spite of the very different geometry of these cations compared with the previously used $[XR_4]^+$ organic ones. Interestingly, this approach has led to a novel structural phase in which the bimetallic extended layers are eclipsed with respect to each other, forming hexagonal tunnels in which the organometallic cations are located. The perfect stacking of these bimetallic layers is in sharp contrast to the structural features found in the $[XR_4]^+$ derivatives, which very often exhibit disordered stackings. This should be advantageous in the characterization of the magnetic structures of these phases by neutron diffraction.

The most interesting feature of this family comes from the hybrid character of these materials: ferro- or ferrimagnetic layers of the type $[M^{II}M^{III}(ox)]^-$ alternate with layers of dia- or paramagnetic species ($[CoCp_2^*]^+$ or $[FeCp_2^*]^+$, respectively). This provides the opportunity to study how the magnetic properties of these multilayered hybrid magnets are affected by the mutual interactions between the two kinds of magnetic layers. In this context we have found that the two layers are quasiindependent, as demonstrated by ESR spectroscopy. This technique has shown the appearance of the signals associated with the two magnetic sublattices. As a consequence, the bulk properties of these magnets have not been significantly affected by the insertion of a paramagnetic layer of $S = 1/2$ spins in between the extended layers. In fact, the critical temperatures remain, within experimental error, unchanged even when comparing $[MCp_2^*]^+$ derivatives with $[XR_4]^+$ analogues. However, the presence of the paramagnetic layer has been shown to have some influence on the hysteresis loops of these compounds. In the same context, a second aspect of interest has been to study the spin polarization in the paramagnetic layers arising from the internal magnetic field created by the bimetallic layers in the ordered state. This polarization has been demonstrated by Mössbauer and ESR spectroscopy. Thus, in the Mössbauer spectra the broad band associated with the paramagnetic cation $[FeCp_2^*]^+$ tends to split into a sextet when the temperature is lowered below T_c, although fast relaxation processes prevent clear observation of the hyperfine spectrum. Clearer evidence of the spin polarization of the Fe^{III} ions has been observed by ESR spectroscopy. A significant g-shift of the signals assigned to

0947-6539/00/0603-0560 $ 17.50+.50/0 *Chem. Eur. J.* **2000**, *6*, No. 3

$[FeCp_2^*]^+$ towards low field has been observed in the ordered state. This demonstrates that below T_c the $S = ½$ spin of the metallocene complex undergoes a Zeeman splitting in presence of a magnetic field that is the sum of the applied and internal fields.

Finally, it is important to stress that this hybrid approach can now be extended to other cationic electroactive species with interesting electronic or optical properties (such as molecular bistability, luminescence, or photochromism) that can be inserted in these oxalate-based magnetic phases in order to create multifunctional molecular materials.

Experimental Section

Materials: The precursor salts $K_3[M^{III}(ox)_3]\cdot 3H_2O$ ($M^{III} = Cr$, Fe) and $[FeCp_2^*][BF_4]$ were prepared according to the literature methods.[15, 16] $[CoCp_2^*][PF_6]$, $MnCl_2\cdot 4H_2O$, $FeSO_4\cdot 7H_2O$, $Co(NO_3)_2\cdot 6H_2O$, $Cu(NO_3)_2\cdot 3H_2O$, and $Zn(NO_3)_2\cdot 6H_2O$, were used as purchased.

$[FeCp_2^*][MnCr(ox)_3]$ (1): An aqueous solution (20 mL) of $K_3[Cr(ox)_3]\cdot 3H_2O$ (1.2 g, 2.4 mmol) and $MnCl_2\cdot 4H_2O$ (2.5 g, 12.6 mmol) was added dropwise to $[FeCp_2^*][BF_4]$ (1 g, 2.4 mmol) dissolved in warm distilled water (150 mL). Immediately, a green precipitate appeared. After the solution was left to stand at room temperature for 30 min, it was filtered in vacuo, washed with water (3×100 mL), and dried at room temperature. Yield: 1.4 g, 83.7 %; $H_{30}C_{26}O_{12}CrMnFe$ (697.3): calcd H 4.35, C 44.78, Cr 7.46, Mn 7.88, Fe 7.96; found H 4.32, C 44.73, Cr 7.50, Mn 7.88, Fe 8.00. Crystals suitable for X-ray diffraction were obtained by slow diffusion of an aqueous solution (30 mL) of $[FeCp_2^*][BF_4]$ (0.1 g, 0.24 mmol) into an aqueous solution (30 mL) of $K_3[Cr(ox)_3]\cdot 3H_2O$ (0.12 g, 0.24 mmol) and $MnCl_2\cdot 4H_2O$ (0.25 g, 1.26 mmol) in a U-shaped tube after 6 months.

$[FeCp_2^*][FeCr(ox)_3]$ (2): This compound was prepared as green microcrystals as described above for **1** but with $FeSO_4\cdot 7H_2O$ (3.6 g, 12 mmol) instead of $MnCl_2\cdot 4H_2O$. Yield: 1.3 g, 77.6 %; $H_{30}C_{26}O_{12}CrFe_2$ (698.2): calcd H 4.34, C 44.72, Cr 7.45, Fe 16.00; found H 4.40, C 44.74, Cr 7.60, Fe 16.20.

$[FeCp_2^*][CoCr(ox)_3]$ (3): This compound was prepared as green microcrystals as described above for **1** but with $Co(NO_3)_2\cdot 6H_2O$ (3.6 g, 12 mmol) instead of $MnCl_2\cdot 4H_2O$. Yield: 1.2 g, 72.3 %; $H_{30}C_{26}O_{12}CrFeCo$ (701.3): calcd H 4.32, C 44.53, Cr 7.46, Fe 7.96, Co 8.41; found H 4.42, C 44.61, Cr 7.50, Fe 8.02, Co 8.28.

$[FeCp_2^*][CuCr(ox)_3]$ (4): This compound was prepared as green microcrystals as described above for **1** but with $Cu(NO_3)_2\cdot 3H_2O$ (3.0 g, 12 mmol) instead of $MnCl_2\cdot 4H_2O$. Yield: 1.0 g, 59.0 %; $H_{30}C_{26}O_{12}CrFeCu$ (705.9): calcd H 4.29, C 44.24, Cr 7.37, Fe 7.91, Cu 9.01; found H 4.39, C 44.35, Cr 7.51, Fe 8.01, Cu, 9.30.

$[FeCp_2^*][ZnCr(ox)_3]$ (5): This compound was prepared as green microcrystals as described above for **1** but with $Zn(NO_3)_2\cdot 6H_2O$ (7.5 g, 25 mmol) instead of $MnCl_2\cdot 4H_2O$. Yield: 1.3 g, 76.5 %; $H_{30}C_{26}O_{12}CrFeZn$ (707.7): calcd H 4.28, C 44.12, Cr 7.46, Fe 7.96, Zn 9.24; found H 4.31, C 44.18, Cr 7.47, Fe 7.98, Zn 9.28.

$[FeCp_2^*][MnFe(ox)_3]$ (6): An aqueous solution (20 mL) of $K_3[Fe(ox)_3]\cdot 3H_2O$ (1.2 g, 2.4 mmol) and $MnCl_2\cdot 4H_2O$ (2.5 g, 12.6 mmol) was added dropwise to $[FeCp_2^*][BF_4]$ (1 g, 2.4 mmol) dissolved in warm distilled water (150 mL). Immediately, a pale green precipitate appeared. After the solution was left to stand at room temperature for 30 min, it was filtered in vacuo, washed with water (3×100 mL), and dried at room temperature. Yield: 0.9 g, 53.5 %; $H_{30}C_{26}O_{12}Fe_2Mn$ (701.2): calcd H 4.32, C 44.54, Mn 7.84, Fe 15.94; found H 4.38, C 44.60, Mn 7.90, Fe 16.30, Co 9.28. Crystals suitable for X-ray diffraction were obtained by slow diffusion in the dark of an aqueous solution (30 mL) of $[FeCp_2^*][BF_4]$ (0.1 g, 0.24 mmol) into an aqueous solution (30 mL) of $K_3[Fe(ox)_3]\cdot 3H_2O$ (0.12 g, 0.24 mmol) and $MnCl_2\cdot 4H_2O$ (0.25 g, 1.26 mmol) in a U-shaped tube after 6 months.

$[FeCp_2^*][FeFe(ox)_3]$ (7): This compound was prepared as green microcrystals as described above for **6** but with $FeSO_4\cdot 7H_2O$ (3.6 g, 12 mmol) instead of $MnCl_2\cdot 4H_2O$. Yield: 1.4 g, 83.1 %; $H_{30}C_{26}O_{12}Fe_3$ (702.1): calcd H 4.32, C 44.48, Fe 23.87; found H 4.40, C 44.60, Fe 24.02.

$[FeCp_2^*][ZnFe(ox)_3]$ (8): This compound was prepared as green microcrystals as described above for **6** but with $Zn(NO_3)_2\cdot 6H_2O$ (7.5 g, 25 mmol) instead of $MnCl_2\cdot 4H_2O$. Yield: 1.4 g, 82.0 %; $H_{30}C_{26}O_{12}Fe_2Zn$ (711.6): calcd H 4.26, C 43.88, Fe 15.70, Zn 9.19; found H 4.29, C, 43.90, Fe 15.74, Zn 9.21.

$[CoCp_2^*][MnCr(ox)_3]$ (9): $[CoCp_2^*][PF_6]$ (1.2 g, 3.6 mmol) was dissolved in dimethylformamide (DMF, 30 mL). This solution was added to an aqueous solution (30 mL) of $K_3[Cr(ox)_3]\cdot 3H_2O$ (1.2 g, 2.4 mmol) and $MnCl_2\cdot 4H_2O$ (2.5 g, 12.6 mmol). After several minutes a yellow precipitate appeared that was filtered in vacuo, washed with water (3×50 mL) and DMF (2×50 mL), and dried at room temperature. Yield: 1.21 g, 71.4 %; $H_{30}C_{26}O_{12}CrMnCo$ (700.4): calcd H 4.34, C 44.58, Cr 7.42, Mn 7.84, Co 8.41; found H 4.36, C 44.72, Cr 7.47, Mn 7.89, Co 8.43.

$[CoCp_2^*][FeCr(ox)_3]$ (10): This compound was prepared as green microcrystals as described above for **9** but with $FeSO_4\cdot 7H_2O$ (3.6 g, 12 mmol) instead of $MnCl_2\cdot 4H_2O$. Yield: 1.5 g, 89.1 %; $H_{30}C_{26}O_{12}CrFeCo$ (701.3): calcd H 4.32, C 44.53, Cr 7.41, Fe 7.96, Co 8.40; found H 4.37, C 44.61, Cr 7.51, Fe 8.10, Co 8.56.

$[CoCp_2^*][CoCr(ox)_3]$ (11): This compound was prepared as green microcrystals as described above for **9** but with $Co(NO_3)_2\cdot 6H_2O$ (3.6 g, 12 mmol) instead of $MnCl_2\cdot 4H_2O$. Yield: 0.7 g, 38.5 %; $H_{30}C_{26}O_{12}CrCo_2$ (704.4): calcd H 4.30, C 44.33, Cr 7.38, Co 16.73; found H 4.33, C 44.47, Cr 7.44, Co 16.90.

$[CoCp_2^*][CuCr(ox)_3]$ (12): This compound was prepared as green microcrystals as described above for **9** but with $Cu(NO_3)_2\cdot 3H_2O$ (3.0 g, 12 mmol) instead of $MnCl_2\cdot 4H_2O$. Yield: 0.9 g, 52.9 %; $H_{30}C_{26}O_{12}CrCoCu$ (709.0): calcd H 4.27, C 44.04, Cr 7.33, Co 8.31, Cu 8.96; found H 4.36, C 44.20, Cr 7.38, Co 8.33, Cu 9.01.

$[CoCp_2^*][ZnCr(ox)_3]$ (13): This compound was prepared as green microcrystals as described above for **9** but with $Zn(NO_3)_2\cdot 6H_2O$ (7.5 g, 25 mmol) instead of $MnCl_2\cdot 4H_2O$. Yield: 1.4 g, 83.2 %; $H_{30}C_{26}O_{12}CrCoZn$ (710.8): calcd H 4.26, C 43.93, Cr 7.32, Co 8.29, Zn 9.20; found H 4.32, C 44.18, Cr 7.45, Co 8.37, Zn 9.28.

$[CoCp_2^*][MnFe(ox)_3]$ (14): An aqueous solution (30 mL) of $K_3[Fe(ox)_3]\cdot 3H_2O$ (1.2 g, 2.4 mmol) and $MnCl_2\cdot 4H_2O$ (2.5 g, 12.6 mmol) was added to $[CoCp_2^*][PF_6]$ (1.2 g, 3.6 mmol) dissolved in DMF (30 mL). After several minutes a yellow precipitate appeared. It was filtered in vacuo, washed with water (3×50 mL) and DMF (2×49 mL), and dried at room temperature. Yield: 0.7 g, 41.4 %; $H_{30}C_{26}O_{12}MnFeCo$ (704.2): calcd H 4.30, C 44.34, Mn 7.80, Fe 7.93, Co 8.37; found H 4.36, C 44.40, Mn 7.86, Fe 7.96, Co 8.37.

$[CoCp_2^*][FeFe(ox)_3]$ (15): This compound was prepared as green microcrystals as described above for **14** but with $FeSO_4\cdot 7H_2O$ (3.6 g, 12 mmol) instead of $MnCl_2\cdot 4H_2O$. Yield: 1.00 g, 59.1 %; $H_{30}C_{26}O_{12}Fe_2Co$ (705.1): calcd H 4.30, C 44.28, Fe 15.84, Co 8.36; found H 4.39, C 44.39, Fe 15.90, Co 8.35.

$[CoCp_2^*][ZnFe(ox)_3]$ (16): This compound was prepared as green microcrystals as described above for **14** but with $Zn(NO_3)_2\cdot 6H_2O$ (7.5 g, 25 mmol) instead of $MnCl_2\cdot 4H_2O$. Yield: 1.3 g, 75.8 %; $H_{30}C_{26}O_{12}FeCoZn$ (714.7): calcd H 4.24, C 43.69, Fe 7.81, Co 8.25, Zn 9.15; found H 4.32, C 43.80, Fe 7.95, Co 8.29, Zn 9.18.

X-ray data collection and analysis: Two green prismatic crystals of **1** and **6** were collected from the U-shaped tubes in which the diffusion had been carried out, and were mounted on a CAD4 Enraf–Nonius diffractometer. Unit cell parameters were determined by a least-squares refinement of the setting angles of 25 independent reflections for both crystals. Similar unit cells were obtained, indicating that both crystals were isostructural, but data collection (ω scan technique) was performed only for **6** because of its better quality. Three standard reflections were measured every 2 h and showed no significant decay. Lorentzian, polarization, and semiempirical absorption corrections (ψ scan method) were applied to the intensity data. Selected experimental parameters and crystal data are reported in Tables 3 and 4. The space group was determined to be *C*2/*m*. All calculations were performed in a SPARC Station 20 (Sun Microsystems). The structure was solved by direct methods with the SIR92[17] program and refined on *F* with the SHELXL-93 program (G. M. Sheldrick, University of Göttingen, 1993). In the structure solution the atoms belonging to the anionic network and to the cations were readily obtained, and after successive Fourier differences even the hydrogen atoms from the methyl groups of the decamethylferrocenium cations were found without any disorder. Because of its high symmetry in the anionic network only one metallic atom, in a special position, was found corresponding to ½Mn and ½Fe. The decamethylfer-

Table 3. Crystallographic data and structural resolution for $[FeCp_2^*][MnFe(ox)_3]$.

formula	$H_{30}C_{26}MnFe_2O_{12}$
size [mm]	$0.1 \times 0.1 \times 0.3$
molecular weight	701.14
T [K]	293(2)
λ [Å]	0.71069
crystal system	monoclinic
space group	$C2/m$
a [Å]	9.063(8)
b [Å]	17.143(3)
c [Å]	9.215(4)
α [°]	90.0
β [°]	93.66(2)
γ [°]	90.0
V [Å^3]	1429(1)
Z	2
ρ_{calcd} [g cm^{-3}]	1.630
$\mu(Mo_{K\alpha})$ [cm^{-1}]	14.99
$F(000)$	718
2Θ limit	4.42 – 63.92
reflections/unique	1909/1871
$I > \sigma(I)$	6
reflections/parmeters	1434/131
goodness-of-fit	1.263
R_1[a]	0.0509
R_2[b]	0.1492
max. dif. peak-hole	0.341 and −0.400

[a] $R_1 = \Sigma(F_o - F_c)/\Sigma(F_o)$. [b] $R_2 = [\Sigma[\omega(F_o^2 - F_c^2)^2]/\Sigma[\omega(F_o^2)^2]]^{1/2}$; $\omega = 1/[\sigma^2(F_o^2) + (0.0343\,P)^2 + 2.4502\,P]$; $P = (F_o^2 + 2F_c^2)/3$.

Table 4. Atomic coordinates and isotropic thermal parameters for $[FeCp_2^*][MnFe(ox)_3]$.

Atom	x	y	z	U (Å^2)
Mn1[b]	1.0000	0.34027(3)	0.5000	0.0289(2)[a]
Fe1[b]	1.0000	0.34027(3)	0.5000	0.0289(2)[a]
Fe2	0.5000	0.5000	1.0000	0.0226(2)[a]
O1	0.8148(3)	0.32159(12)	0.6218(2)	0.0384(5)[a]
O2	0.6192(3)	0.24245(11)	0.6290(2)	0.0365(5)[a]
O3	1.0788(3)	0.43461(12)	0.6267(2)	0.0378(5)[a]
C1	0.7321(5)	0.5000	0.9909(5)	0.0368(11)[a]
C2	0.6121(4)	0.5412(2)	1.1892(3)	0.0322(6)[a]
C3	0.6857(4)	0.5669(2)	1.0659(3)	0.0365(7)[a]
C4	0.8182(8)	0.5000	0.8561(7)	0.071(2)[a]
C5	0.5515(6)	0.5933(3)	1.3017(5)	0.0647(14)[a]
C6	0.7182(8)	0.6500(3)	1.0282(7)	0.072(2)[a]
C7	1.0462(4)	0.5000	0.5732(4)	0.0283(8)[a]
C8	0.7318(3)	0.26861(14)	0.5738(3)	0.0282(6)[a]
H1	0.9239(78)	0.5000	0.8894(67)	0.066(19)
H2	0.7809(76)	0.5402(37)	0.7923(68)	0.151(29)
H3	0.6013(68)	0.5967(32)	1.3814(61)	0.092(18)
H4	0.5250(70)	0.6431(34)	1.2672(62)	0.109(21)
H5	0.4625(60)	0.5694(26)	1.3290(53)	0.076(15)
H6	0.6534(60)	0.6793(28)	1.0770(57)	0.081(18)
H7	0.7215(82)	0.6550(36)	0.9247(80)	0.137(26)
H8	0.8018(83)	0.6621(38)	1.0631(75)	0.123(28)

[a] Atoms refined anisotropicaly. $U_{eq} = (4/3)[a^2B(1,1) + b^2B(2,2) + c^2B(3,3) + ab(\cos\gamma)B(1,2) + ac(\cos\beta)B(1,3) + bc(\cos\alpha)B(2,3)]$. [b] Disordered atoms with occupancy factor = 0.5.

rocenium complex is in its staggered configuration, with local symmetry D_{5d}. All atoms (except hydrogens) were refined anisotropically without any further disorder. Crystallographic data (excluding structure factors) for the structure reported in this paper have been deposited with the Cambridge Crystallographic Data Centre as supplementary publication no. CCDC-182551. Copies of the data can be obtained free of charge on application to CCDC, 12 Union Road, Cambridge CB2 1EZ, UK (fax: (+44) 1223-336-033; e-mail: deposit@ccdc.cam.ac.uk).

Magnetic properties: Variable-temperature DC susceptibility measurements were carried out on polycrystalline samples in the temperature range 2 – 300 K at a magnetic field of 0.1 T. The susceptibility data were corrected for the diamagnetic contributions calculated from Pascal's constant tables. Variable-temperature AC susceptibility measurements were carried out in the temperature range 2 – 50 K, with an alternating applied field of 3.95 G at different frequencies (1 – 1500 Hz). Hysteresis loops were measured between 5 and −5 T. All of these measurements were carried out with a magnetometer (Quantum Design MPMS-XL-5) equipped with a SQUID sensor.

ESR spectroscopy: ESR measurements were performed over the range 4.2 – 300 K with an X-band spectrometer (Bruker 200D) equipped with a liquid helium cryostat.

Mössbauer spectroscopy: Mössbauer spectra were recorded with a ^{57}Co/Rh source in a constant acceleration spectrometer equipped with a liquid helium cryostat. The spectra were fitted to Lorentzian lines by a nonlinear minimization iterative routine.

Acknowledgments

We thank The Ministerio de Educación y Cultura (MEC) and The Generalitat Valenciana (GV) for financial support to purchase a SQUID magnetometer. This work was supported by the MEC (Grant MAT98-0880). We are also grateful for financial help from the "Materialwissenschaftliches Forschungszentrum der Universität Mainz" and the "Fonds der Chemischen Industrie". J.R.G.M. thanks the GV for a predoctoral fellowship.

[1] a) *Molecular Magnetism: From Molecular Assemblies to the Devices*, NATO ASI Series, *Vol. E321* (Eds.: E. Coronado, P. Delhaès, D. Gatteschi, J. S. Miller), Kluwer, Dordrecht, **1996**; b) J. S. Miller, *Adv. Mater.* **1990**, *2*, 98.

[2] a) Z.-J. Zhong, N. Matsumoto, H. Okawa, S. Kida, *Chem. Lett.* **1990**, 87; b) M. Ohba, H. Tamaki, N. Matsumoto, H. Okawa, S. Kida, *Chem. Lett.* **1991**, 1157.

[3] H. Tamaki, Z.-J. Zhong, N. Matsumoto, S. Kida, M. Koikawa, N. Achiwa, Y. Hashimoto, H. Okawa, *J. Am. Chem. Soc.* **1992**, *114*, 6974.

[4] a) H. Tamaki, M. Mitsumi, K. Nakamura, N. Matsumoto, S. Kida, H. Okawa, S. Iijima, *Chem. Lett*. **1992**, 1975; b) H. Okawa, N. Matsumoto, H. Tamaki, M. Ohba, *Mol. Cryst. Liq. Cryst.* **1993**, *233*, 257; c) J. Larionova, B. Mombelli, J. Sanchiz, O. Kahn, *Inorg. Chem.* **1998**, *37*, 679.

[5] a) C. Mathonière, S.-G. Carling, D. Yusheng, P. Day, *J. Chem. Soc. Chem. Commun.* **1994**, 1551; b) C. Mathonière, J. Nuttall, S.-G. Carling, P. Day, *Inorg. Chem.* **1996**, *35*, 1201.

[6] a) R. Pellaux, H.-W. Schmalle, R. Huber, P. Fisher, T. Hauss, B. Ouladdiaf, S. Decurtins, *Inorg. Chem.* **1997**, *36*, 2301; b) S. Decurtins, H.-W. Schmalle, H.-R. Oswald, A. Linden, J. Ensling, P. Gütlich, A. Hauser, *Inorg. Chim. Acta* **1994**, *216*, 65; c) L.-O. Atovmyan, G.-V. Shilov, R.-N. Lyubovskaya, E.-I. Zhilyaeva, N.-S. Ovanesyan, S.-I. Pirumova, I.-G. Gusakovskaya, *JETP Lett.* **1993**, *58*, 766.

[7] E. Coronado, J.-R. Galán-Mascarós, C. Giménez-Saiz, C.-J. Gómez-García, C. Ruiz-Perez, S. Triki, *Adv. Mater.* **1996**, *8*, 737.

[8] a) A.-W. Graham, M. Kurmoo, P. Day, *J. Chem. Soc. Chem. Commun.* **1995**, 2061; b) M. Kurmoo, A.-W. Graham, P. Day, S.-J. Coles, M.-B. Hursthouse, J.-L. Caulfield, J. Singleton, F.-L. Pratt, W. Hayes, L. Ducasse, P. Guionneau, *J. Am. Chem. Soc.* **1995**, *117*, 12209.

[9] E. Coronado, J.-R. Galán-Mascarós, C.-J. Gómez-García, *Synth. Metals* **1999**, *102*, 1459.

[10] a) Z. Gu, O. Sato, T. Iyoda, K. Hashimoto, A. Fujishima, *Mol. Cryst. Liq. Cryst.* **1996**, *286*, 147; b) S. Bernard, P. Yu, T. Coradin, E. Rivière, K. Nakatani, R. Clément, *Adv. Mater.* **1997**, *9*, 981.

[11] M. Clemente-León, E. Coronado, J.-R. Galán-Mascarós, C.-J. Gómez-García, *Chem. Commun.* **1997**, 1727.

[12] L. Néel, *Ann. Phys. (Paris)* **1948**, *3*, 137.

[13] a) S. Iijima, F. Mizutani, *Mol. Cryst. Liq. Cryst.* **1997**, *306*, 227; b) S. Iijima, F. Mizutani, M. Mitsunmi, N. Matsumoto, H. Okawa, *Inorg. Chim. Acta* **1996**, *253*, 47; c) S. Iijima, T. Katsura, H. Tamaki, M. Mitsumi, N Matsumoto, H. Okawa, *Mol. Cryst. Liq. Cryst.* **1993**, *233*, 263.

[14] Mössbauer spectra for the decamethylcobaltocenium derivative also confirm the different temperature-dependent magnetization for the two sublattices.

[15] J.-C. Baylar, E.-M. Jones in *Inorganic Synthesis*, *Vol. 1* (Ed.: H. S. Booth), McGraw–Hill, New York, **1939**, pp. 35.

[16] D. Hendrickson, Y. Son, H. Gray, *Inorg. Chem.* **1971**, *10*, 1559.

[17] A. Altomare, G. Cascarano, C. Giacovazzo, A. J. Guagliardi, *Appl. Crystallogr.* **1994**, *27*, 1045.

Received: May 17, 1999 [F1784]